Coulomb-induced emission dynamics and self-consistent calculations of type-II Sb-containing quantum dot systems

K. Gradkowski,[1,2,*] T. J. Ochalski,[1,2,†] N. Pavarelli,[1,2] H. Y. Liu,[3] J. Tatebayashi,[4] D. P. Williams,[1,2] D. J. Mowbray,[5] G. Huyet,[1,2] and D. L. Huffaker[6]

[1]*Tyndall National Institute, University College Cork, Cork, Ireland*

[2]*Centre for Advanced Photonics and Process Analysis, Cork Institute of Technology, Cork, Ireland*

[3]*Department of Electronic and Electrical Engineering, University College London, Torrington Place, London WC1E 7JE, United Kingdom*

[4]*Institute for Nano Quantum Information Electronics, University of Tokyo, 4-6-1 Komaba, Meguro-ku, Tokyo 153-8505, Japan*

[5]*Department of Physics and Astronomy, University of Sheffield, Sheffield S3 7RH, United Kingdom*

[6]*Department of Electrical Engineering, California NanoSystems Institute, University of California, Los Angeles, California 90095, USA*

(Received 8 December 2011; revised manuscript received 5 January 2012; published 20 January 2012)

This paper investigates the effects of Coulomb interactions on the emission dynamics of Sb-containing quantum dot (QD) systems under high excitation densities. Two different type-II confinements are studied: confined electrons with unconfined holes using InAs/GaAs QDs capped with a GaAsSb quantum well (type-IIa), and confined holes with unconfined electrons using GaSb/GaAs QDs capped with an InGaAs quantum well (type-IIb). Time-resolved photoluminescence experiments are compared with self-consistent numerical calculations using an 8-band $\mathbf{k}\cdot\mathbf{p}$ model. In both structures, we observe a significant blueshift of emission and wavelength-dependent radiative lifetimes, but with marked quantitative differences between the two systems: in the type-IIa, the blueshift is 12 meV with a change in lifetime from 1.4 ns to 2.0 ns, and in the type-IIb, the blueshift is 63 meV with lifetime change from 100 ps to 23 ns. We present a comprehensive explanation of all the important features of the experimental data in terms of Coulomb-induced changes to the carrier wave functions and confining potentials, with the separate confinement of the electrons and holes being a crucial factor.

DOI: 10.1103/PhysRevB.85.035432 PACS number(s): 78.47.D−

I. INTRODUCTION

The advantages of semiconductor quantum dots (QDs) are by now well known.[1–4] The employment of type-II band alignment, in which the electrons and holes are spatially separated due to the lack of a confining potential for one of the carrier types, can have several added benefits over the more conventional (i.e., type-I) heterostructures, for example in a hybrid quantum dot–quantum well (QW) design.[5] Additionally, type-II heterostructures in III-V semiconductors are typically created by the inclusion of antimony, which lowers the band gap. This is an excellent starting point for long-wavelength applications such as gas sensing and solar cells.[6–9] Another possible employment of type-II QDs is in memory cells,[10,11] where the storage time has been estimated to be on the scale of years.

Depending on which of the carrier species is confined to the QD, we can have a type-IIa, where the confined (0D) electrons are surrounded by unbound holes (2D or 3D), or a type-IIb system, for the opposite situation. The former has been primarily studied with respect to InP/GaAs heterostructures.[12–14] However, it can be produced in the standard InAs/GaAs QD system when the dots are capped by a GaAsSb QW of sufficient antimony concentration. Using this method one can obtain emission at 1.6 μm.[15,16] Type-IIb quantum dot systems are more commonly found in the literature, since they are inherent in GaAsSb/GaAs QDs, even for a low antimony content.[17–21] For Sb-rich QDs the emission wavelength can theoretically reach 1.7–2.0 μm,[5] which is nearly the same as that of bulk GaSb. By employing other nanostructures, such as an InGaAs QW, one can reduce the transition energy even further.[5,21] The quantum well additionally increases the carrier capture cross-section and confines the electrons to the plane of the QD layer, although with associated intermixing difficulties.[22,23]

Extensive studies of these systems have uncovered interesting emission properties. Photoluminescence (PL) experiments yielded a blueshift of the emission spectra with increasing pump excitation density.[24–26] This result has not been rigorously reproduced theoretically.[24,26–29] Lasers produced from GaSb/GaAs QDs likewise have shown a pronounced blueshift before reaching lasing threshold.[30] Time-resolved photoluminescence (TRPL) measurements performed on type-IIa QD structures yielded the trend that with increasing power density the lifetimes became shorter.[31,32] A similar trend has been observed for type-IIb systems, but with much longer lifetimes of the order of tens of nanoseconds.[25,29,33]

The experimental results present in the literature were explained in terms of Coulomb interactions, but the employed models were somewhat simplified—usually considering a spherical QD in an effective mass approximation.[34–36] These works also did not include the dependence of the properties on the excitation density. Additionally, no studies have compared the type-II subtypes.

In this work we present a systematic and comprehensive study of the dynamic emission properties of both type-II QD configurations and explain the experimentally observed phenomena using a single model based on self-consistent $\mathbf{k}\cdot\mathbf{p}$ calculations. While our approach has itself several simplifications, it takes into account a nonideal dot shape, more typical of realistic QDs, as well as a multiple, interacting valence band structure. It also accounts for dynamic alterations to the wave function shapes when subjected to carrier injection.

II. EXPERIMENTAL METHOD AND RESULTS

We have studied and compared both type-II QD cases, grown by molecular-beam epitaxy (MBE). The type-IIa structure consisted of QDs formed on a GaAs substrate by depositing 2.8 monolayers (MLs) of InAs, followed by a 6 nm $GaAs_{0.82}Sb_{0.18}$ QW and then 100 nm of GaAs.[15,16,31] The type-IIb system consisted of GaSb/GaAs QDs and was grown by depositing 4 MLs of GaSb on GaAs. These dots are then overgrown with 7 nm of $In_{0.2}Ga_{0.8}As$ and finally covered with 100 nm of GaAs.[19,20]

To study the emission dynamics of the QDs, we employed a streak camera system equipped with an IR-enhanced thermo-electrically cooled photocathode. The structures were placed in a closed-cycle helium cryostat and cooled to 7–8 K. Because of the wide range of decay lifetimes we have utilized two modes of excitation. For the fast dynamics a 780 nm, 300 fs Ti:sapphire laser operating at 75.6 MHz has been used. This can achieve energies of 13.2 nJ per pulse, which allows for very high excitation densities. For long lifetimes a 780 nm pulsed laser diode operating at 1 MHz has been employed with energies per pulse in the range of 10 fJ.

Figure 1 shows emission dynamics of the type-IIa QDs. We can distinguish three radiative transition channels. When there are few carriers in the structure, the ground state (GS) emission occurs at 0.992 eV. At $t = 0$, when the carrier density in the structure is the highest, the maximum of this emission is blueshifted by about 12 meV. As the carrier density decreases over time, the relaxation of the GS emission to its few-carrier position (indicated in the figure by the black line) is initially rapid, becoming more gradual as the carriers are depleted. Similar features are observable for the first excited state (ES1). Its final peak position is around 1.055 eV, but at $t = 0$ it is blueshifted by about 8 meV. The second excited state (ES2) is also visible around 1.117 eV.

Further details of the emission dynamics of the type-IIa QD system can be obtained by extracting the decay traces

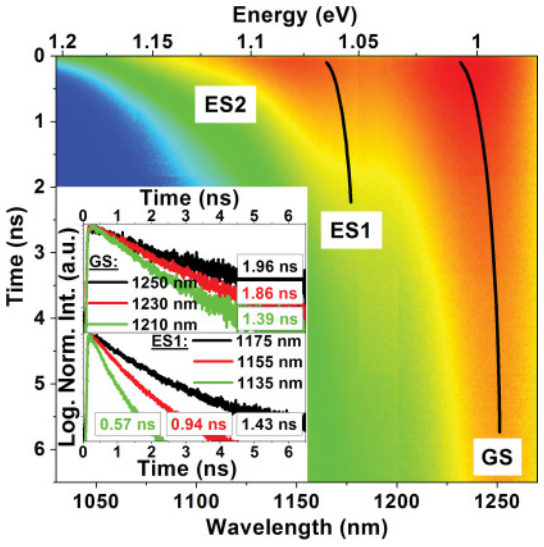

FIG. 1. (Color online) Logarithmic plot of the emission dynamics of the type-IIa QD structure. Black lines show the temporal evolution of the peak position of ground and excited states. Inset depicts the decay traces at different wavelengths for ground and excited states.

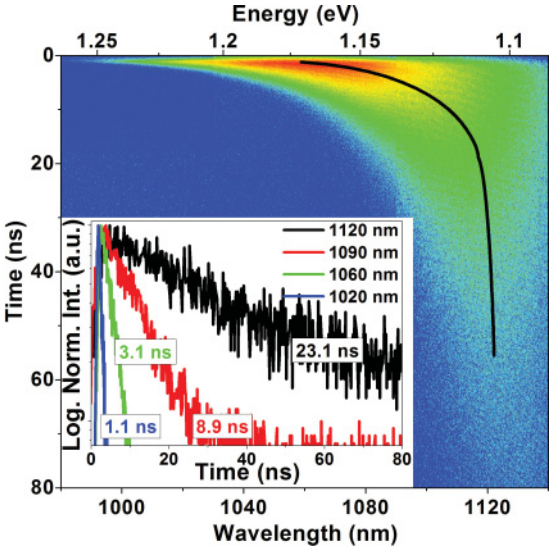

FIG. 2. (Color online) Logarithmic plot of the emission dynamics of the type-IIb QD structure. Black line shows the temporal evolution of the peak position of the ground state. Inset depicts the decay traces at different wavelengths.

at different wavelengths for each emission state (inset in Fig. 1). We observe that the high-energy component of each channel exhibits shorter lifetimes than the low-energy tail. Sufficiently accurate decay times can be extracted by fitting each decay trace with a single exponential function. For the GS, at 1.025 eV the decay lifetime is 1.39 ns, and increases to 1.86 ns at 1.008 eV and to 1.96 ns at 0.992 eV, which is longer than the typical values of 1 ns for conventional type-I InAs QDs.[37] The ES1 transition behaves similarly, but with greater changes of the carrier lifetimes: 0.57 ns at 1.092 eV, 0.94 ns at 1.075 eV, and 1.43 ns at 1.055 eV.

The emission dynamics of the type-IIb QD structure are presented in Fig. 2. Instead of several distinct optical transitions, we observe only one, albeit very broad, feature. Immediately after the excitation pulse the spectrum covers nearly 150 meV and has a maximum around 1.163 eV. Over time it narrows significantly and exhibits a redshift to the low carrier density emission energy of 1.1 eV. The magnitude of the emission shift, depicted in Fig. 2 as a black line, is much greater than the one observed for the type-IIa QD structure and is around 60 meV. Similar to the type-IIa system, the radiative lifetimes are also wavelength dependent and increase for lower energies (see inset in Fig. 2). The timescale range is however much wider, covering decay times from hundreds of picoseconds to tens of nanoseconds.[38]

III. THEORETICAL MODEL

A. Model details

To describe the Coulomb interactions in type-II QD systems, which are responsible for the observable dynamic emission features, we require a model that can approximate as closely as possible the real band structure of quantum dots of a given shape and yet be simple enough to easily allow for a self-consistent calculation. In our work we employ an 8-band $\mathbf{k}\cdot\mathbf{p}$ formalism. We take the explicit form of the

Hamiltonian from Refs. 39 and 40, and the material parameters from Ref. 41. We solve the Hamiltonian by using a Fourier-transform method.[42] An advantage of this approach, besides computational simplicity, is that the QD properties enter the Hamiltonian only via its characteristic function, $\chi_{QD}(\boldsymbol{r})$, which returns 1 inside the dot, and 0 outside. For a number of dot shapes there are analytical solutions for the Fourier transform of this function.[42–44] This allows for an accurate account of the shape and size of the dot in the simulation, which will have an influence on the modification of the band structure due to strain.

Similarly, the optical matrix elements, which are proportional to the optical transition probability, are calculated as Fourier coefficients of the bulk matrix elements because of our choice of basis functions:[39,40]

$$M_{n',n}(\vec{k}) = \left| \langle n',\vec{k}|\vec{e}\cdot\frac{\partial \hat{H}}{\partial \vec{k}}|n,\vec{k}\rangle \right|^2, \tag{1}$$

where $\vec{e} = (e_x, e_y, e_z)$ is the light polarization vector. In this work we choose it to be unitary along the x axis to simulate the conditions of the experiment, where the emission is collected from a narrow angle centered on the z axis perpendicular to the growth plane of the dots.

To evaluate the influence of the carrier injection on the optical properties of the system we need to calculate the correction each injected particle brings to the band structure. Toward this goal we employ Coulomb potentials, where we treat the wave functions of the electron and hole particles as densities of negative and positive charge, respectively (Hartree-Fock approach). The Coulomb interaction is included in the Hamiltonian as

$$\left(H_0 + \sum_{\sigma} V^{(\sigma)}(r)\right)\Psi = E\,\Psi, \tag{2}$$

where H_0 is the single-particle Hamiltonian, $V^{(\sigma)}$ is the Coulomb potential due to the state σ, and the sum is over all occupied states. The coefficients of the Fourier transform of $V^{(\sigma)}$ are calculated by transforming the Poisson equation, where the value for the relative permittivity is taken as that of the matrix material, GaAs, throughout. This method is further described in Ref. 45, where we have adapted it for the 3D confinement.

Since our goal is to find charge-density-dependent energy levels and wave functions we construct a self-consistent algorithm. We parameterize the number of injected electron-hole pairs per dot as q. We take the eigenvector solutions of the unperturbed Hamiltonian and we populate the energy levels with particles for which we calculate the corresponding Coulomb potentials. In the QD we always fill the lowest available states. This approximation is supported by the fact that the experiment is performed at 7 K, where the possibility of thermionic emission is small, as well as by the type-II nature of the optical transition, which enforces long radiative lifetimes and promotes a formation of quasiequilibrium before the next radiative event. The situation for the QW will be regarded for each case separately.

The sum of all the considered Coulomb potentials gives us a correction to be added to the neutral energy band profile in the next iteration. The algorithm then proceeds until the changes to the level energies upon subsequent steps are smaller than a certain threshold. In our case we have placed this threshold at 0.2 meV, which is 1/3 of the thermodynamic energy at the temperature at which the experiment is performed.

The average dot density of 4×10^{10} cm^{-2} provides a dot spacing, and hence an in-plane super-cell (SC) size, of 50 nm. The SC height was set to 30 nm to ensure proper boundary conditions. The dot's shape was assumed to be a truncated pyramid, which is commonly found in these structures.[19,46–48] The dot size was determined using atomic-force microscopy (AFM) and transmission electron microscopy (TEM) and the composition was established in corroboration with the experiment by meticulous testing of various configurations. Thus the type-IIa QDs are 16 nm × 16 nm in base size, 4 nm in height, and contain ∼90% In. For the type-IIb structure, the QDs are 15 nm × 15 nm base size, 8 nm in height, and contain ∼20% Sb. The dots are capped with a QW of appropriate thickness and composition: 6 nm $GaAs_{0.82}Sb_{0.18}$ for the type-IIa structure and 7 nm $In_{0.2}Ga_{0.8}As$ QW for the type-IIb system. In the latter case, since the simulated dot is higher than the well, we have to take into consideration that the QW material slightly overgrows the QD, which can be plainly seen in the TEM cross-section images.[19,20] We thus allow for the well to overgrow the dot by 3 nm by creating an InGaAs layer on top the GaSb QD [see inset in Fig. 3(b)].

B. Band structure

Figure 3(a) presents the calculated band structure of the type-IIa QD system. The conduction band (CB) contains six doubly (spin) degenerate levels confined inside the QD. Due to the symmetry of the dot in the x-y direction the first excited electron state is further degenerate and we will treat it as one. The valence band (VB) edge for the quantum well is 36 meV above the edge of the dot. The first confined hole state is in the QW and lies 18 meV above the first confined state of the QD, which is enough to prevent significant mixing of the QD and QW states.

Red arrows in Fig. 3 show possible optical transitions. We have several possibilities to examine in order to determine the final carrier states under excitation, which will be used for the self-consistent simulations. In this case we may have a competition between the intradot recombination of type-I nature (0De-0Dh) and type-II emission between the electrons in the dot and holes in the well (0De-2Dh). Any holes that are created in the barrier material will most likely relax into the GaAsSb QW. Through phonon-assisted scattering they will thermalize to the lowest available energy levels. Therefore, if the states in the well above those of the dot (in terms of the energy scale of Fig. 3) are unoccupied the hole can transfer there before recombining. At low temperature the probability of exciting into the dot states is minimal as there is insufficient thermal energy to activate this process.

The number of available states in the QW can be ascertained by a simple calculation based on the density of states (ρ_{2D}) equation

$$N = \int_{E_{QW}}^{E_{QD}} \rho_{2D}(E)\,dE = \frac{Sm^*}{\pi\hbar^2}\,|\Delta E|, \tag{3}$$

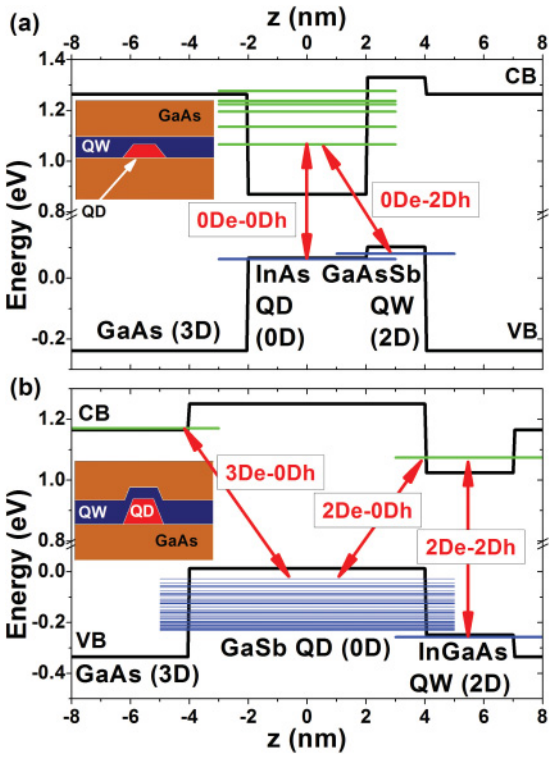

FIG. 3. (Color online) Calculated band profiles along the z axis ($x = y = 0$) of the (a) type-IIa and (b) type-IIb QD system for the parameters in text. Arrows show possible optical transitions. The insets show the x-z band profile in the plane $y = 0$ in the simulation environment.

where m^* is the effective mass of the particle, S is the SC surface area, and $|\Delta E|$ is the spacing between the ground QW and QD states (E_{QW} and E_{QD}, respectively). We establish that in this energy spacing we can have 90 holes per SC, which is a much greater number than the total confined electron states in the QD. Therefore in the self-consistent calculation we place the electrons on the single-particle QD states, and all the holes on the first state inside the well.

Figure 3(b) presents the calculated band structure of the type-IIb QD system. The barrier height for the electrons is 85 meV, while the hole confinement potential is 350 meV. Due to this, and to the fact that the holes possess a large effective mass, there are many confined hole states in the dot [Fig. 3(b) depicts the first 100], while the electrons are outside in the QW. This situation determines the dominant type-II transition channel [2De-0Dh red arrow in Fig. 3(b)] for this structure. The large dot population immediately suggests that the Coulomb interactions in this structure will play a much greater role than in the case of the type-IIa structure, which has a maximum of only 12 particles inside the QD. Using Eq. (3) we calculate that we can place 70 electrons per SC in the QW before reaching the GaAs band edge, which we set as our limit for the purpose of the self-consistent calculations.

C. Evolution of single-particle wave functions

Figure 3 depicts the band structures under no excitation conditions. When populated with carriers according to previously described rules, the Coulomb interactions will modify

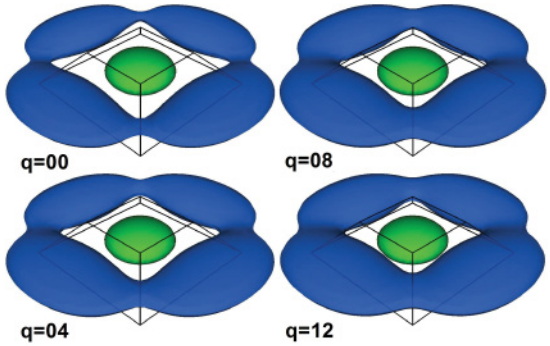

FIG. 4. (Color online) Calculated evolution of the GS hole wave function (blue, outside the dot) as a function of excitation density in the type-IIa structure. The GS electron wave function (green, inside the dot) is provided as reference.

the confinement potential. The difference in confinement dimensionalities leads to the carriers inside the small volume of the dot strongly repelling each other and attracting the carriers outside. The interactions among the carriers outside are much weaker because of their lower charge density. This mechanism is responsible for the dynamic evolution of the emission properties of the type-II QD structures.

The local modification of the confinement potential will result in a modification of the single-particle wave functions to fit the new potential. In Fig. 4 we present this mechanism for the type-IIa structure. The GS hole wave function (blue) resides in the QW, while the electron GS (green) is in the QD. We observe that with increasing charge density (q), the holes move closer to the dot. This shift is not very large, because the QD forms an effective barrier for the holes. We can also see that, due to the symmetry of the dot shape, the hole wave function prefers to occupy the faces of the QD. For the electrons, their wave function shapes will be altered by the repulsion between them and as a result they will spread evenly in all directions. These changes are however minuscule in comparison with those for the holes.

In Fig. 5 we present the evolution of the GS electron wave function for the type-IIb structure. The GS hole has been provided as a reference and, for clarity, three adjacent SCs are shown. The maximum number of calculated e-h pairs in the simulation is much greater than for the type-IIa structure since there are more available QD states. This means that the magnitude of the wave function modification will be more significant as well. When the dot is empty ($q = 0$) any electrons will preferentially remain in the well between the dots. When we start to inject carriers into the system the Coulomb attraction brings the electrons closer to the dot and eventually, for high excitation densities ($q = 70$), they form a tight ring at the slopes of the pyramid. The large number of available hole states in the dot will also lead to a significant modification of the wave functions as is shown in the zooms in Fig. 5. The repulsion will act to push the holes outward, expanding them into the wider base of the QD.

In the two cases, the qualitative difference between the wave functions of the carriers outside the QD (the 2D wave functions) at $q = 0$ can be explained by the fact that the potential step between the QD and the QW for the holes in the type-IIa structure is very small (see Fig. 3).

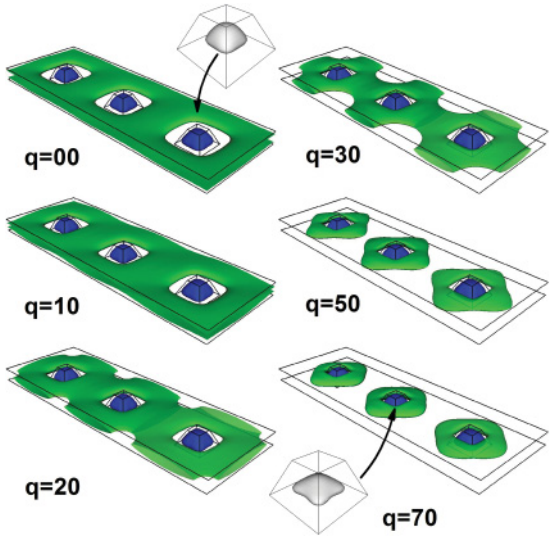

FIG. 5. (Color online) Calculated evolution of the GS electron wave function (green, outside the dots) as a function of excitation density in the type-IIb structure. The GS hole wave function (blue, inside the dot) is provided as a reference. The images depict three adjacent SCs for clarity. Zooms show the shape of the hole wave function for selected charge densities.

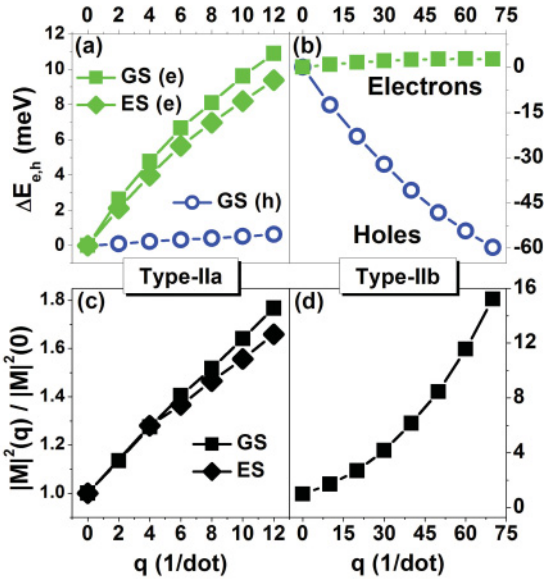

FIG. 6. (Color online) Calculated charge-density-dependent evolution of single-particle electron and hole levels of the (a) type-IIa and (b) type-IIb structures, while (c) and (d) depict calculated optical matrix elements for corresponding transition channels.

This means that strain-induced potential modifications are the dominant influence in this case, providing a shallow confinement potential for the holes near the dot. This is not present for the electrons in the type-IIb case, and in any event the strain-induced modifications are dominated by the larger potential step in this case. Consequently, the hole wave functions in the type-IIa structure are confined close to the sides of the pyramid, while in the type-IIb structure the electrons are spread throughout the QW, avoiding the dot.

D. Evolution of the optical transition properties

The local modification of the confinement potential and the resulting change of the wave function shapes affect the optical properties of the structure, such as the transition energy and probability. Figures 6(a) and 6(b) depict charge-density-dependent evolution of the energy levels in the type-IIa and type-IIb structures, respectively. In both these systems, competing interactions between electron-hole, electron-electron, and hole-hole can lead to complex behavior; however, the overall trends are governed by a dominant interaction.

For the type-IIa structure we show explicitly only the first two (doubly spin degenerate) electron states (green closed symbols) as well as the first hole level (blue open circles). We observe that the repulsion between the electrons occupying the QD leads to a reduction of the confining potential, which translates into pushing the levels up and out of the QD. For the GS the maximum calculated value of the shift is 11 meV when the dot is full. For the first ES the maximum shift is 9 meV. The holes on the other hand are attracted toward the dot by the electrons, thus increasing their confinement. However the corresponding energy shift is tiny (less than 1 meV), because the modification of the (unperturbed) valence band edge [see Fig. 3(a)] is relatively small.

For the type-IIb structure the experiment yields only a single, broad feature;[38] thus for theoretical consideration we are most interested in the evolution of the electron and hole ground states. The large number of available hole levels means that the energy changes are much more significant than in the type-IIa system. The total calculated hole shift is about 60 meV; meanwhile the electrons experience only a very small shift of ∼3 meV.

The difference in the rates of change of energy between electrons and holes causes the observed blueshift of the transition energy with increasing charge density. For the type-IIa structure the maximum calculated shift for the ground and first excited states is 10 and 8 meV, respectively. For conventional type-I InAs/GaAs QDs, the presence of the holes inside the dot compensates for the interelectron Coulomb repulsion and the transition energy does not change significantly, although this can be different when the dot is subjected to a very large excitation densities.[49] For the type-IIb structure the total shift is 63 meV, much larger than in the type-IIa. Furthermore, in the type-IIa scheme the shift will be terminated abruptly by saturating the confined states inside the QD. In the type-IIb case the multitude of available dot levels allows for a large change in the emission wavelength. The approach to the maximum achievable shift, determined by the total number of confined states, is more gradual because the density of states increases near the continuum of the well. Also, the wave functions of these higher levels are less confined, leading to a lower charge density and hence a smaller contribution to the Coulomb potential.

The modification of the wave function shapes during carrier injection also has an impact on the optical transition probability, which is proportional to the overlap between the constituent carrier wave functions. We can see that for both type-II QD systems the wave functions of the carriers which are confined to the dot are modified less profoundly than those

of the carriers outside it. The calculated changes to the optical matrix element are presented in Figs. 6(c) and 6(d) for the type-IIa and type-IIb systems, respectively. In the type-IIa structure the increasing confinement of the holes around the QD and the expansion of the electron wave functions due to Coulomb interactions lead to a sublinear increase of the matrix elements. The total enhancement factor for the GS is around 1.75 for $q = 12$. The matrix element evolution in the type-IIb structure likewise shows that with increasing injection we observe enhancement of the optical transition probability, calculated to be $\sim$15 for $q = 70$, a value an order of magnitude greater than in the case of the type-IIa structure. This is caused by the difference in nature of the type-IIa and type-IIb systems, where in the latter case we can place more carriers inside the dot, which enhances the magnitude of the Coulomb interactions.

IV. DISCUSSION

By combining the theoretical charge-density dependencies of the optical properties of the structures from Fig. 6, we can make a comparison to the experimental results. This is presented in Figs. 7 and 8. Squares represent the experimental values of the decay time, whereas lines are the radiative lifetimes calculated from the optical matrix element between the constituent carrier wave functions, as described in Ref. 1. It should be noted that these calculated radiative lifetimes do not give the total decay lifetime, which will also include contributions from, e.g., nonradiative lifetimes and intradot relaxation processes. Given the low temperature of the current experiments, these additional contributions will be quite small, as evidenced by the reasonable fit to experiment.

For the type-IIa structure (Fig. 7) we can see that the calculations can satisfactorily explain the observable emission dynamics. All radiative states undergo a redshift with decreasing charge density, as explained earlier. The magnitude of the energy shift taken from the experiment is very close to the one determined by the calculation: 12 meV and 10 meV for ground and excited state, respectively. The increment of the radiative lifetimes during the course of the experiment is dictated by the evolution of the optical matrix element. This is at a maximum at $t = 0$ (high charge density), when the overlap is increased by

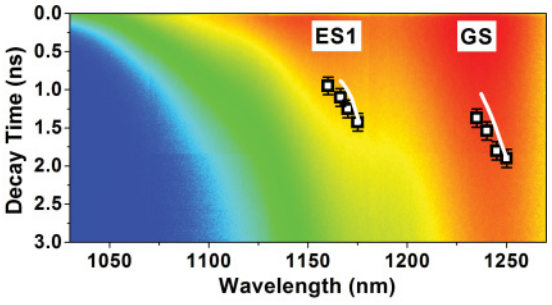

FIG. 7. (Color online) Comparison between experimentally (black squares) and theoretically determined (white lines) lifetimes presented as a function of the emission wavelength (combination of the data in Fig. 6) for type-IIa structure.

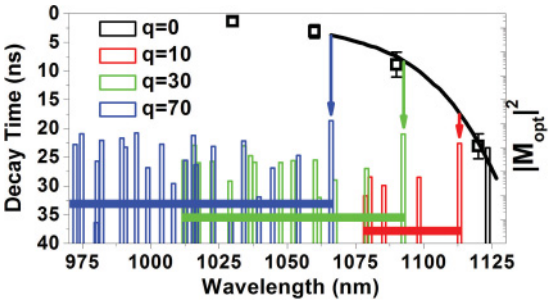

FIG. 8. (Color online) Comparison between experimentally (black squares) and theoretically determined (black line) lifetimes presented as a function of the emission wavelength for type-IIb structure (see Fig. 2). Vertical bars represent the values of the optical matrix element for several values of q and arrows indicate the GS position for given q. Horizontal bars show the span of possible emissive states for the corresponding charge densities.

the proximity of the holes to the dot, and then relaxes toward the neutral state as charge density decreases.

For the type-IIb structure (Fig. 8) we observe that the theory is in excellent agreement with the experiment. The total width of the spectrum (see Fig. 2) cannot be however attributed solely to the shift of the GS. Vertical bars in Fig. 8 represent optical matrix elements for transitions between the electron QW state and the confined hole QD states at a specific carrier density. Those levels, when the structure is under excitation, shift with the GS and their transition probability is also enhanced relative to the GS. The higher-energy states, when populated with holes, can become effective channels of radiative recombination,[38] resulting in a very wide spectrum after the pump pulse (depicted as horizontal bars in Fig. 8).

This also explains the fast spectral narrowing. After the laser pulse excites the structure and carriers thermalize to their lowest available states, the carrier density is at its highest. This means that the spectrum is very broad (many radiative channels), blueshifted, and with short decay times. The many recombination events in the structure however quickly depopulate the valence band. Thus, in a very short time, the spectrum experiences a large redshift, the number of radiative states is reduced, and the radiative processes slow down. With lower Coulomb interactions the subsequent radiative events will take longer until only the ground state is populated and the slowest red component of the spectrum is achieved. This mechanism accounts for the nonlinear behavior of the emission dynamics observed in this system.

V. CONCLUSIONS

In this work we have investigated the effects of Coulomb interactions on the dynamic optical properties of type-II quantum dot systems based on GaSb. By utilizing TRPL and comparing the experimental results to theoretical calculations based on a self-consistent 8-band $\mathbf{k}\cdot\mathbf{p}$ algorithm, we were able to interpret the Coulomb-driven mechanisms of band-gap renormalization. We have shown that the observed blueshift with increasing injected carrier density is caused largely by a Coulomb-induced shift of the band edge within the dot, which predominantly affects only the charge type which is confined

there. The evolution of the decay time scales on the other hand is caused by the modification of the wave functions of the carriers outside the QD. Between the two type-II systems there are nevertheless significant differences in the emission dynamics, which stem from the differences in densities of states for confined holes and electrons in the two systems.

ACKNOWLEDGMENTS

This work was supported by the European Union under Marie Curie Actions (Contract No. 041985), Science Foundation Ireland (Contract No. 07/IN.1/I929), and INSPIRE under the HEA PRTLI4 program.

*Current address: Institute of Chemistry, Hebrew University of Jerusalem, Givat Ram, 91904 Jerusalem, Israel.

†Corresponding author: tomasz.ochalski@tyndall.ie

[1]D. Bimberg, M. Grundmann, and N. N. Ledentsov, *Quantum Dot Heterostructures* (Wiley, New York, 1999).

[2]R. J. Young, S. J. Dewhurst, R. M. Stevenson, A. J. Shields, P. Atkinson, K. Cooper, and D. A. Ritchie, Appl. Phys. Lett. **91**, 011114 (2007).

[3]L. O. Mereni, V. Dimastrodonato, R. J. Young, and E. Pelucchi, Appl. Phys. Lett. **94**, 223121 (2009).

[4]F. Chi, X.-N. Dai, and L.-L. Sun, Appl. Phys. Lett. **96**, 082102 (2010).

[5]K. Gradkowski, T. J. Ochalski, D. P. Williams, J. Tatebayashi, A. Khoshakhlagh, G. Balakrishnan, E. P. O'Reilly, G. Huyet, L. R. Dawson, and D. L. Huffaker, J. Lumin. **129**, 456 (2009).

[6]R. B. Laghumavarapu, A. Moscho, A. Khoshakhlagh, M. El-Emawy, L. F. Lester, and D. L. Huffaker, Appl. Phys. Lett. **90**, 173125 (2007).

[7]A. Krier and V. V. Sherstnev, J. Phys. D: Appl. Phys. **33**, 101 (2000).

[8]A. Krier, M. Stone, Q. D. Zhuang, P.-W. Liu, G. Tsai, and H. H. Lin, Appl. Phys. Lett. **89**, 091110 (2006).

[9]P.-W. Liu, G. Tsai, H. H. Lin, A. Krier, Q. D. Zhuang, and M. Stone, Appl. Phys. Lett. **89**, 201115 (2006).

[10]M. Geller, A. Marent, T. Nowozin, and D. Bimberg, J. Phys. Condens. Matter **20**, 454202 (2008).

[11]B. Marquardt, M. Geller, A. Lorke, D. Reuter, and A. D. Wieck, Appl. Phys. Lett. **95**, 022113 (2009).

[12]F. Iikawa, M. P. F. Godoy, M. K. K. Nakaema, M. J. S. P. Brasil, M. Z. Maialle, M. A. Degani, E. Ribeiro, G. Medeiros-Ribeiro, W. Carvalho Jr., and J. A. Brum, Brazil. J. Phys. **34**, 555 (2004).

[13]P. F. Gomes, M. P. F. de Godoy, G. O. Dias, F. Iikawa, M. J. S. P. Brasil, M. A. Cotta, and J. R. Madureira, J. Phys. D: Appl. Phys. **43**, 045303 (2010).

[14]J. R. Madureira, M. P. F. de Godoy, M. J. S. P. Brasil, and F. Iikawa, Appl. Phys. Lett. **90**, 212105 (2007).

[15]H. Y. Liu, M. J. Steer, T. J. Badcock, D. J. Mowbray, M. S. Skolnick, P. Navaretti, K. M. Groom, M. Hopkinson, and R. A. Hogg, Appl. Phys. Lett. **86**, 143108 (2005).

[16]H. Y. Liu, M. J. Steer, T. J. Badcock, D. J. Mowbray, M. S. Skolnick, F. Suarez, J. S. Ng, M. Hopkinson, and J. P. R. David, J. Appl. Phys. **99**, 046104 (2006).

[17]E. R. Galser, B. R. Bennett, B. V. Shanabrook, and R. Magno, Appl. Phys. Lett. **68**, 3614 (1996).

[18]R. A. Hogg, K. Suzuki, K. Tachibana, L. Finger, K. Hirakawa, and K. Arakawa, Appl. Phys. Lett. **72**, 2856 (1998).

[19]J. Tatebayashi, A. Khoshakhlagh, S. H. Huang, L. R. Dawson, G. Balakrishnan, and D. L. Huffaker, Appl. Phys. Lett. **89**, 203116 (2006).

[20]J. Tatebayashi, A. Khoshakhlagh, S. H. Huang, G. Balakrishnan, L. R. Dawson, D. L. Huffaker, D. A. Bussian, H. Htoon, and V. Klimov, Appl. Phys. Lett. **90**, 261115 (2007).

[21]K. Gradkowski, T. J. Ochalski, D. P. Williams, S. B. Healy, J. Tatebayashi, G. Balakrishnan, E. P. O'Reilly, G. Huyet, and D. L. Huffaker, Phys. Status Solidi B **246**, 752 (2009).

[22]C. Jiang and H. Sakaki, Physica E **26**, 180 (2005).

[23]C. Jiang and H. Sakaki, Physica E **32**, 17 (2006).

[24]F. Hatami, N. N. Ledentsov, M. Grundmann, J. Böhrer, F. Heinrichsdorff, M. Beer, D. Bimberg, S. S. Rivumov, P. Werner, U. Gösele, J. Heydenreich, U. Richter, S. V. Ivanov, B. Ya. Meltser, P. S. Kop'ev, and Zh. I. Alferov, Appl. Phys. Lett. **67**, 656 (1995).

[25]C.-K. Sun, G. Wang, J. E. Bowers, B. Brar, H.-R. Blank, H. Kroemer, and M. H. Pilkuhn, Appl. Phys. Lett. **68**, 1543 (1996).

[26]D. Alonso-Álvarez, B. Alén, J. M. García, and J. M. Ripalda, Appl. Phys. Lett. **91**, 263103 (2007).

[27]K. Suzuki, R. A. Hogg, and Y. Arakawa, J. Appl. Phys. **85**, 8349 (1999).

[28]N. N. Ledentsov, J. Böhrer, M. Beer, F. Heinrichsdorff, M. Grundmann, D. Bimberg, S. V. Ivanov, B. Ya. Meltser, S. V. Shaposhnikov, I. N. Yassievich, N. N. Faleev, P. S. Kop'ev, and Zh. I. Alferov, Phys. Rev. B **52**, 14058 (1995).

[29]F. Hatami, M. Grundmann, N. N. Ledentsov, F. Heinrichsdorff, R. Heitz, J. Böhrer, D. Bimberg, S. S. Ruvimov, P. Werner, V. M. Ustinov, P. S. Kop'ev, and Zh. I. Alferov, Phys. Rev. B **57**, 4635 (1998).

[30]J. Tatebayashi, A. Khoshakhlagh, S. H. Huang, G. Balakrishnan, L. R. Dawson, D. L. Huffaker, D. A. Bussian, H. Htoon, and V. Klimov, Appl. Phys. Lett. **90**, 261115 (2007).

[31]Y. D. Jang, T. J. Badcock, D. J. Mowbray, M. S. Skolnick, J. Park, D. Lee, H. Y. Liu, M. J. Steer, and M. Hopkinson, Appl. Phys. Lett. **92**, 251905 (2008).

[32]Y.-A. Liao, W.-T. Hsu, P.-C. Chiu, J.-I. Chyi, and W.-H. Chang, Appl. Phys. Lett. **94**, 053101 (2009).

[33]J. Tatebayashi, B. L. Liang, R. B. Laghumavarapu, D. A. Bussian, H. Htoon, G. Balakrishnan, L. R. Dawson, and D. L. Huffaker, Nanotechnology **19**, 295704 (2008).

[34]J. M. Rorison, Phys. Rev. B **48**, 4643 (1993).

[35]U. E. H. Laheld, F. B. Pedersen, and P. C. Hemmer, Phys. Rev. B **48**, 4659 (1993).

[36]U. E. H. Laheld, F. B. Pedersen, and P. C. Hemmer, Phys. Rev. B **52**, 2697 (1995).

[37]E. Harbord, P. Spencer, E. Clarke, and R. Murray, Phys. Rev. B **80**, 195312 (2009).

[38]K. Gradkowski, N. Pavarelli, T. J. Ochalski, D. P. Williams, J. Tatebayashi, G. Huyet, E. P. O'Reilly, and D. L. Huffaker, Appl. Phys. Lett. **95**, 061102 (2009).

[39]A. T. Meney, B. Gonul, and E. P. O'Reilly, Phys. Rev. B **50**, 10893 (1994).

[40]S. Tomic, E. P. O'Reilly, R. Fehse, S. J. Sweeney, A. R. Adams, A. D. Andreev, S. A. Choulis, T. J. Hosea, and H. Riechert, IEEE J. Sel. Top. Quantum Electron. **9**, 1228 (2003).

[41]I. Vurgaftman, J. R. Meyer, and L. R. Ram-Mohan, J. Appl. Phys. **89**, 5815 (2001).

[42]A. D. Andreev and E. P. O'Reilly, Phys. Rev. B **62**, 15851 (2000).

[43]A. D. Andreev, J. R. Downes, D. A. Faux, and E. P. O'Reilly, J. Appl. Phys. **86**, 297 (1999).

[44]D. P. Williams, A. D. Andreev, E. P. O'Reilly, and D. A. Faux, Phys. Rev. B **72**, 235318 (2005).

[45]S. B. Healy and E. P. O'Reilly, IEEE J. Quantum Electron **42**, 608 (2006).

[46]H. Eisele, O. Flebbe, T. Kalka, C. Preinesberger, F. Heinrichsdorff, A. Krost, D. Bimberg, and M. Dähne-Prietsch, Appl. Phys. Lett. **75**, 106 (1999).

[47]P. Kratzer, Q. K. K. Liu, P. Acosta-Diaz, C. Manzano, G. Costantini, R. Songmuang, A. Rastelli, O. G. Schmidt, and K. Kern, Phys. Rev. B **73**, 205347 (2006).

[48]H. Eisele, A. Lenz, R. Heitz, R. Timm, M. Dähne, Y. Temko, T. Suzuki, and K. Jacobi, J. Appl. Phys. **104**, 124301 (2008).

[49]K. Gradkowski, T. J. Ochalski, N. Pavarelli, D. P. Williams, G. Huyet, B. Liang, and D. L. Huffaker, Appl. Phys. Lett. **97**, 091105 (2010).